Check for updates

Corrosion protection mechanism of Ce^{4+}/organic inhibitor for AA2024 in 3.5% NaCl

Mohamed Gobara, [*a] Ahmad Baraka,[a] Robert Akid[b] and Mahmoud Zorainy[ac]

Cerium is a rare earth element that has been widely proposed for the corrosion protection of aluminium alloys (AA). Both cerium salts, Ce^{3+} and Ce^{4+}, have been used in combination with other compounds to offer synergistic inhibition, however, the inhibitive corrosion mechanism when using Ce^{4+} with organic compounds is still not clear. In this study, the synergistic inhibition effect of Ce^{4+} and melamine (M) on the corrosion of aluminium alloy 2024 (AA2024) in 3.5% NaCl solution was investigated. Potentiodynamic Polarization (PDP) and Electrochemical Impedance Spectroscopy (EIS) techniques were used to study the synergistic effect of different Ce^{4+}/M ratios on the corrosion behaviour of AA2024. The PDP study showed that a combination of 50% Ce^{4+} and 50% M leads to the lowest corrosion rates, both acting as cathodic inhibitors. Both PDP and EIS results indicated that M or Ce^{4+} in isolation did not offer effective corrosion protection, while the combination of M and Ce^{4+} significantly enhances the corrosion protection with a synergism parameter equal to 3.5. SEM and EDX observations confirm the findings from the electrochemical techniques. XPS was used to investigate the mechanism of protection, revealing that the reduction of Ce^{4+} to Ce^{3+} occurs during protection of AA2024. A new mechanism of corrosion synergistic inhibition by Ce^{4+} and organic compounds is postulated where the role of the organic compounds is to enhance the reduction of Ce^{4+}.

1. Introduction

Aluminium is considered as the second most used metal in engineering applications. The continuous growth of aluminium consumption, especially in the fields of transport, engineering and packaging can be attributed to several of its properties, such as ease of recycling, low density, diversity of aluminium alloys and suitability for surface treatments.[1]

Aluminium alloy 2024 (AA2024) is perhaps the alloy that has been most widely used in aircraft applications.[2] The main alloying element of this alloy is copper, being added at 3.8–4.9%.[3] The high strength/weight ratio and good fatigue resistance of this alloy is a consequence of the presence of fine intermetallic particles (IMP). The IMPs are classified into three categories according to their size: (1) hardening precipitates (<0.1 μm), (2) dispersoids (0.01–0.1 μm) and (3) Inclusions (>1 μm). Although the latter do not provide a major contribution to the mechanical properties, they have a significant impact on the localized corrosion susceptibility of the alloy.[4] The localised corrosion includes pitting and stress corrosion cracking[5] where the IMP act as active cathodic sites accelerating corrosion of the aluminium matrix.[6,7]

A great deal of research and product development has been conducted to overcome this drawback including, mechanistic studies on conversion and organic coatings, and inhibitors.[8–12] Whilst many inhibitors have been used to control the corrosion of aluminium alloys, only a few of them can be used in industry due to restrictions derived from environmental legislation, most notably the ban on Cr(VI) systems. In order to reduce the environmental impact of chemical inhibitors, effective synergism is an important approach to decrease the concentration of chemicals within an inhibitor. This approach entails using a combination of inhibiting compounds whose effect is greater than the sum of any of the individual compounds. It can be achieved by the interaction between components of the inhibitor and/or between the inhibitor and ion(s) present in the solution.[13] The synergistic effect between organic–inorganic combinations has been studied for different alloys and solutions.[14–18] In general, the organic component is responsible for adsorption onto the metal surface through heteroatoms (N, O, S, and P), double/triple bonds or aromatic rings.[19–21]

Cerium salts have been widely used as corrosion inhibitors,[11,22–25] where the essential step of the inhibition mechanism involving cerium species, in an aerated neutral solution, is the formation of insoluble cerium oxides and/or hydroxides on the cathodic sites, where the oxygen reduction reaction is inhibited.[25–27] A number of workers have investigated the synergism of cerium with inorganic[28–31] and organic[8,30,32–34] materials as corrosion inhibitors. Also, the synergistic effect of using

[a]Chemical Engineering Department, Military Technical College, Cairo, Egypt. E-mail: m_gobara@yahoo.com

[b]Department of Materials, The University of Manchester, Manchester, UK

[c]Chemical Engineering Department, École Polytechnique de Montréal, Montreal, Canada

inhibitor anions, such as phosphate, with cerium cations to enhance corrosion inhibition efficiency has been studied.[4,35] However, only a few of these studies has been concerned with the use of Ce^{4+}.[36–40] The role of cerium in the corrosion inhibition process mainly depends on the oxidation state of cerium ion (*i.e.* Ce^{3+} or Ce^{4+}) and the pH of the solution. Generally, the corrosion prevention property of cerium is related to the presence of Ce^{3+}.[41–43] Irrespective of cerium treatment, the prevention mechanism comprises two steps: (1) an insoluble oxide/hydroxide of Ce^{3+} is formed due to interaction with hydroxide ions on the cathodic sites where adequate concentration of OH^- is produced and (2) the formed insoluble Ce compound precipitates on the intermetallic particles.[44–46] Therefore, the cathodic reaction is inhibited and the corresponding anodic reaction significantly reduces. These two steps take more than 24 h to achieve suitable protection.[47] For AA2024 the reduction reaction was suppressed on intermetallic inclusions and it was found that the minimum concentration of Ce^{3+} in neutral NaCl electrolyte is 5 ppm.[48] For all cerium treatments, it can be concluded that the presence of Ce^{3+} is the key role in the protection of aluminium.

The synergistic effect of using Ce^{4+} with organic materials such as corrosion inhibitors has been studied.[36,39,40,49–53] Although, Ce^{3+} was not included in these studies and the crucial step of Ce^{3+} precipitation on the cathodic site was not clear, the inhibition efficiencies were improved by synergism.

Li et al.,[40,49,51] investigated the synergistic effect of using vanillin with Ce^{4+} for corrosion prevention of steel in HCl and H_2SO_4. In another study, iso-vanillin and Ce^{4+} were obtained and used for the corrosion prevention of steel in sulphuric acid.[38] Although, the XPS analysis clearly showed Ce^{3+} on the protected surface (>50% of the cerium components), the authors referred the presence of Ce^{3+} to the reduction of the protective Ce^{4+} film in air which is not feasible and further analyses were required to determine exactly or alternatively how Ce^{3+} is produced. In contrast to this findings, however, no evidence of that interaction with air was detected. In fact, vanillin is highly susceptible to oxidation[54–56] *i.e.* it can be used as a reducing agent, and consequently it may reduce Ce^{4+} to Ce^{3+}.

Further, the synergistic inhibition effect of Ce^{4+} with sodium oleate has been used for corrosion prevention of steel in an acidic solution.[39] The authors proposed that the enhancement in corrosion protection was due to the formation of a Ce^{4+} complex which was adsorbed onto the metal surface forming a protective layer. However, sodium oleate can work as a reducing agent[57,58] by breaking the C=C group.[59]

Another study showed that L-phenylalanine/Ce^{4+} improved the corrosion prevention of copper in HCl solution.[36] The authors also related the corrosion inhibition to the formation of a complex; nevertheless, the ease of oxidation of L-phenylalanine in aqueous solution[60] was not taken in consideration.

Li et al. studied the synergistic inhibition effect of Ce^{4+} with 3,4-dihydroxybenzaldehye on cold rolled steel in sulphuric acid[50] and hydrochloric acid solutions.[61] The corrosion prevention mechanism was based on the formation of a complex between Ce^{4+} and 3,4-dihydroxybenzaldehye.

Although, this hypothesis was built upon the capability of Ce^{4+} to form a complex (*via* vacant orbits 4f, 5d and 6s), no chemical analysis was applied to confirm the composition of the complex. Again, the ease of oxidation of 3,4-dihydroxybenzaldehye[62–65] was not discussed.

Hany[66] also studied the synergistic corrosion inhibition of Ce^{4+} with polyethylene glycols (PEG) on carbon steel in dilute sulphuric acid solution. The author referred the enhancement in the corrosion prevention to the formation of a complex that formed from Ce^{4+} and polyethylene glycols, however, no further analysis was performed to confirm this assumption. Other studies were performed confirming the ease of oxidation of PEG,[67–71] and also that Ce^{4+} can be used to catalyse the oxidation reaction of PEG in sulphuric acid solution.[72,73]

Finally, vanillin, iso-vanillin and 3,4-dihydroxybenzaldehye have been used as electron donors[74] and, they have some activity in presence of Al_2O_3.[75] These properties were not taken in account during these studies.

This current study attempts to understand the potential synergistic effect between melamine and Ce^{4+}, in the form of cerium(IV) sulphate. A novel corrosion inhibitor (SY) consisting of melamine with cerium sulphate was developed for the corrosion resistance of AA2024 in 3.5% NaCl solution. The synergistic effect was investigated based on electrochemical measurements; PDP and EIS. Surface morphology was also studied using an SEM. A corrosion mechanism was postulated based on the results obtained from the electrochemical analysis along with X-ray photoelectron spectroscopy (XPS).

2. Experimental

2.1 Material

Aluminium alloy AA2024 samples were obtained from Q-panels with the following composition:

AA2024	Si	Fe	Cu	Mn	Mg	Cr	Zn	Ti	Al
	0.50	0.50	3.8–4.9	0.30–0.9	1.2–1.8	0.10	0.25	0.15	Remainder

Rectangular coupons of the alloy with dimensions 25 mm × 25 mm × 1 mm were used as the substrate material (working electrode). The surface of the coupon was first ground with 320, 600 and 1200 grit abrasive SiC paper to remove scale and contamination from the surface. The ground specimen were degreased in ethanol then with deionised water then dried by a stream of air for 30 s and kept in an airtight desiccator at room temperature.

All chemicals were used 'as received' without further purification or treatment and all the solutions were prepared with deionized water. Melamine, cerium(IV) sulphate and sodium chloride were obtained from Sigma-Aldrich. The blank corrosive electrolyte was prepared by dissolving NaCl in deionised water forming a 3.5 wt% solution, being representative of artificial sea water. This corrosive solution has been widely used for testing the corrosion resistance of aluminium alloys. Each inhibitor was then added separately to the blank corrosive solution forming different inhibited electrolyte.

2.2 Characterization techniques

All corrosion tests were conducted in a standard one litre three-electrode cell. The sample represents the working electrode; two platinum electrodes were used as the counter electrodes and a saturated calomel electrode (SCE) as the reference electrode. The ohmic contribution was minimized by coupling the SCE to a fine capillary tube that was kept close to the working electrode.

Potentiodynamic polarization (PDP) scans were performed using an initial delay time at steady open-circuit potential (OCP) for 60 min to stabilize the surface. The polarization scan commenced in the cathodic region, scanning positively to anodic region in the potential range of −250 to +250 mV with respect to OCP, at a rate of 0.5 mV s^{-1}.

From the results the inhibition efficiency (IE%) was calculated using eqn (1),:[12]

$$IE\% = \frac{\left(I_{corr}^{\circ} - I_{corr}\right)}{I_{corr}^{\circ}} \times 100 \qquad (1)$$

where: I_{corr}° is the corrosion current density of the blank sample and I_{corr} is the corrosion current density of the inhibited sample.

EIS tests were performed at room temperature in the same electrochemical cell used for potentiodynamic polarization. The EIS tests were performed over a frequency range of 10^5–10^{-2} Hz with 10 mV peak to peak amplitude, using an AC signal at OCP.

A Gamry™ potentiostat/galvanostat, model reference-600 was used for all electrochemical measurements, where, the ratio of corrosive solution volume to sample surface area is not less than 40 ml cm^{-2} for all experiments. The impedance experimental results were fitted to equivalent electrical circuits using the nonlinear least square fitting technique provided by the Gamry™ software.

Each experiment was performed at least three times to ensure reproducibility of the results. The electrochemical experimental results were plotted using SigmaPlot software and uncertainties were calculated and attached to appropriate results.

The morphology and composition of the corroded samples were investigated by scanning electron microscopy (SEM) using a Zeiss-EVO-10, equipped with Energy Dispersive X-ray Spectroscopy (EDX).

Photoelectron spectroscopic (XPS) analysis was performed using a mono-chromated Al K X-ray source (1486.6 eV) typically operated at 10 mA emission current and 10 kV anode potential −100 W. The take-off angle for the photoelectron analyser is 90° and acceptance angle of 30° and the data analysis was carried out using CASAXPS software. The main C 1s peak (284.7 eV) was selected to correct the high resolution scans.[76] Survey scans were run for 10 minutes and high resolution scans were run for between 2–3 minutes depending on the signal. The analysis chamber pressure was better than 5×10^{-9} mmHg. During XPS studies Shirley background subtraction and Gaussian shaped were applied in the XPS spectrum peak fitting procedure.

3. Results and discussion

3.1 Corrosion measurements of AA2024 in 3.5% NaCl solution

The inhibition effect of the novel inhibitor 'SY' on the corrosion behaviour of AA2024 in 3.5% NaCl solution was investigated by two electrochemical techniques; PDP and EIS. To select the optimum ratio of the mix of Ce^{4+} and melamine, the PDP technique was applied and the inhibition efficiency was calculated from the results.

Fig. 1 illustrates the polarization curves of AA2024 with different concentration ratios of melamine to Ce^{+4} at a total concentration of 10 ppm over a potential range of ± 250 mV *versus* OCP showing both cathodic and anodic polarization curves. The blank sample shows the highest corrosion current density with respect to different concentration ratios. Also, it seems that all additives improve the cathodic polarization than the anodic one. The ratio of 50 : 50% melamine to Ce^{+4} appears to have the minimum corrosion current density, I_{corr}.

Fig. 2 shows the inhibition efficiency (*E*%) of the Tafel extrapolation curves. It can be seen that the synergism between melamine and Ce^{4+} ion was revealed. Specifically, the inhibition efficiency for the combination of melamine and Ce^{4+} is much greater than the summation of that for melamine and Ce^{4+} individually. The greatest inhibition efficiency, 90.4 ± 1.8%, was achieved by a blend of 5 ppm Ce^{4+} and 5 ppm melamine which was chosen to represent the SY composition throughout the rest of this study.

To evaluate the synergistic effect of Ce^{4+} and melamine, blank solutions (B), containing either melamine (M), or ceric sulphate (C) were prepared at a concentration of 5 ppm.

The AA2024 samples were separately tested with different inhibitor solutions; M, C, and SY. The typical potentiodynamic polarization curves for different samples as measured in aerated 3.5% NaCl solution are superimposed in Fig. 3. The figure demonstrates anodic and cathodic polarization behaviour of the AA2024. The associated corrosion kinetics
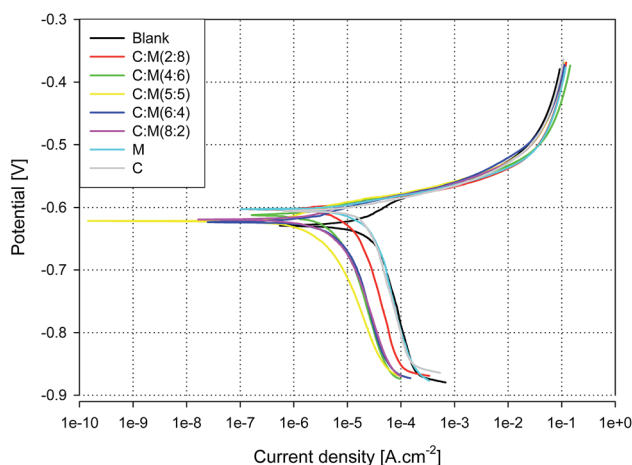

Fig. 1 Tafel curves of AA2024 in 3.5% NaCl at room temperature with different concentration ratios Ce^{4+} to melamine at a total blend concentration of 10 ppm.

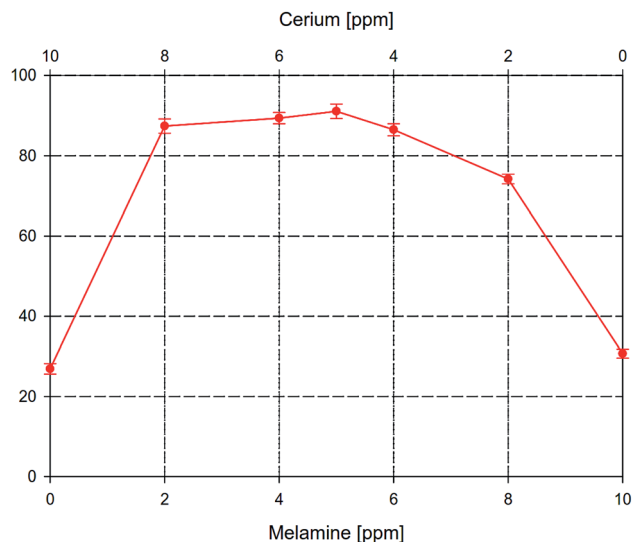Fig. 2 The inhibition efficiency of AA2024 in 3.5% NaCl at room temperature with different concentration ratios Ce^{4+} to melamine.
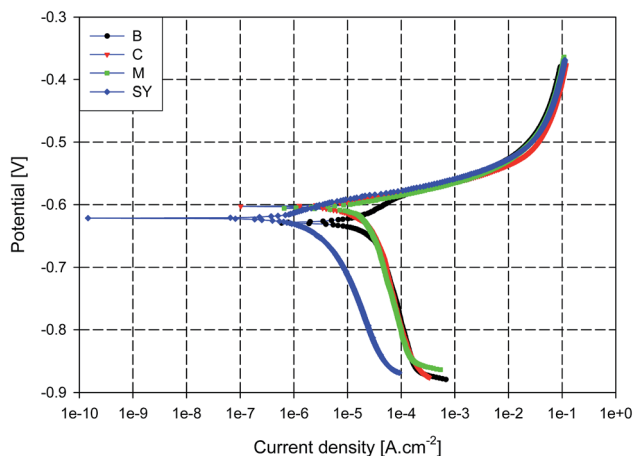

Fig. 4 Nyquist plots for AA2024 after 24 h in 3.5% NaCl solution with different additives at room temperature.

Fig. 3 Tafel plots of AA2024 in 3.5% NaCl solution with different addition at room temperature.

Fig. 5 Phase angle plots for AA2024 in 3.5% NaCl solution with different additives at room temperature.

parameters (E_{corr}, β_c, β_a, I_{corr}, IE%) were determined by extrapolating the cathodic and anodic Tafel lines of each curve.

It can be seen from Fig. 3 that the corrosion current density of SY sample is much smaller than the other three solution conditions. Also, the anodic branch of all samples seems to be identical that the decrease in I_{corr} appears to be due to a decrease in the cathodic current suggesting that SY
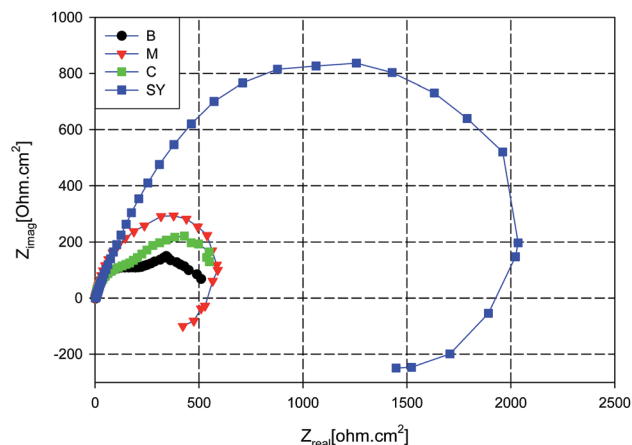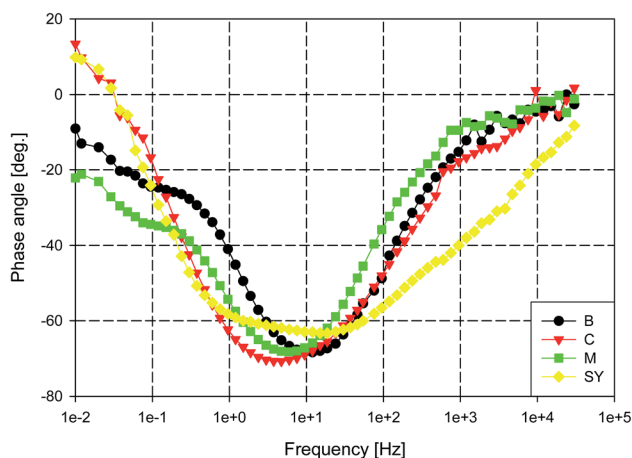
acts as a cathodic type inhibitor.[77–79] Also, samples M and C show little effect on the corrosion behaviour of AA2024 sample where M and C have a typical corrosion current which is marginally smaller than that of B. These results are consistent with previous results[41] where low concentration of Ce^{4+} did not offer corrosion protection for AA2024. For all samples, the current density abruptly increases in the anodic polarization direction beyond the corrosion potential, E_{corr}, and no passive region is observed reflecting the risk of localized corrosion.

Table 1 Corrosion kinetic parameters of AA2024 with different inhibitors

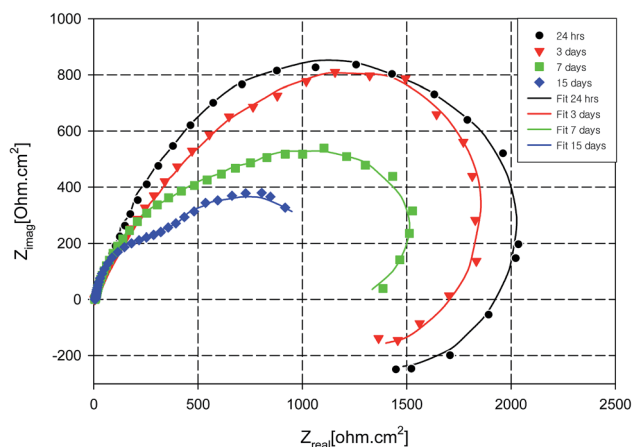| Conc. [ppm]	β_a [mV dec^{-1}]	β_c [mV dec^{-1}]	E_{corr} [mV]	I_{corr} [mA cm^{-2}]	IE%
B	32	248	-629 ± 2	$5.2 \pm 0.3 \times 10^{-5}$	—
M	28	249	-603 ± 4	$3.8 \pm 0.2 \times 10^{-5}$	26.9 ± 1.3
C	25	238	-606 ± 2	$3.6 \pm 0.3 \times 10^{-5}$	30.7 ± 1.5
SY	30	225	-615 ± 3	$0.5 \pm 0.1 \times 10^{-5}$	90.4 ± 1.8

Paper

Fig. 6 Temporal Nyquist plots for AA2024 in 3.5% NaCl solution with SY inhibitor at room temperature.

Table 1 gives the electrochemical kinetic parameters of Tafel extrapolations (E_{corr}, β_c, β_a, I_{corr}, IE%). From the table, the anodic, β_a, and the cathodic, β_c, slopes of all samples are close to each other. This behaviour suggests that the presence of different additives does not affect the mechanism of both anodic and cathodic reactions but changes the rates of corrosion. The table also shows that the corrosion current density (I_{corr}) of SY sample is much smaller than those of other samples. Finally, the addition of Ce^{4+} ion alone does not significantly decrease the corrosion rate of AA2024 alloy which is in a good agreement with previous studies.[49,50]

The synergistic parameter (S) is an expression to compare the expected corrosion rate, when either A or B is present and does not interact, with the experimentally measured rate in the presence of the inhibitor mixture. The mathematical expression of synergism parameter, S, for a mixture of two inhibitors, A and B, is given in eqn (2);[80,81]

$$S = \frac{1 - \eta_A - \eta_B - (\eta_A \eta_B)}{1 - \eta_{(AB)}} \qquad (2)$$

where η_A and η_B are the inhibition efficiencies determined for compounds A and B respectively and η_{AB} is the inhibition efficiency for the mixture A + B (concentrations of A and B in the mixture should be the same as in the corresponding separate situations).[50,53] The synergism between the two substances manifests itself when the value of S is greater than unity, whereas when S is less than unity the synergy is antagonistic.

The value of S was calculated from Table 1 and it was found to be 3.5 indicating ceric sulphate and melamine have a synergistic effect in corrosion prevention of alloy AA2024 in 3.5% NaCl solution.

From the above discussion, it can conclude that AA2024 is susceptible to localized corrosion when immersed in 3.5% NaCl solution. In addition, melamine or Ce^{4+} sulphate solely cannot protect AA2024 from corrosion in that electrolyte.

For a better understanding of the corrosion performance of SY and to confirm the PDP results, electrochemical impedance spectroscopy (EIS) measurements were performed after 24 h of immersion in 3.5% NaCl solution. EIS was conducted for B, C, M and SY samples.

Fig. 4 illustrates the Nyquist plots of AA2024 in aerated 3.5% NaCl at open circuit potential with different additives. In addition, EIS for the blank sample was also presented for comparison. The plots do not show perfect semicircles due to the frequency dispersion and the inhomogeneity of the surface.[82,83] It can be seen that the diameter of the SY Nyquist' semicircle is much greater than for the other additives which indicates that SY affords superior corrosion protection for AA2024 in this electrolyte. Also, the diameters of M and C Nyquist' capacitive loop are slightly greater than that of the blank sample which reflects the slight improvement in the corrosion resistance due to addition of each of them. The figure also shows an inductive behaviour for both M and SY samples. The physical explanation of an inductive loop at low-frequency range is not sufficiently clear; it has been attributed to adsorption processes and/or formation of passive layer and/or redox activity.[84] The inductive loop of the M sample may be due to the relaxation process occurred by adsorption of organic compound, melamine, on the metal surface.[85,86] Also, SY shows an inductive loop at low frequency range which may point to redox activity[7,87] and/or the relaxation process of adsorption. The adsorption process may be attributed to the presence of the organic component, melamine; however the redox activity would be due to the presence of Ce^{4+} which is the candidate undergoing the redox process.

The total diameter of the semicircles can be used to represent the total resistance of the metal with different additives;[88] consequently it is used to calculate the synergistic factor, S, according to eqn (1), where it is equal to 3.4 which is comparable with that of PDP measurements.

The phase plots of these samples are presented in Fig. 5, where B and M samples show a time constant at low frequency
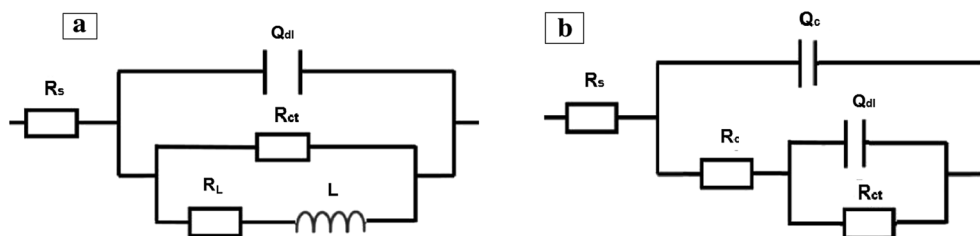

Fig. 7 Typical (a) one-time and (b) two-times constant electrical equivalent circuits used for modelling of impedance data.

Table 2 EIS fitting parameters of AA2024 immersed in 3.5% NaCl solution with different additives

| | R_s [Ω Cm²] | Q_c | | R_c [Ω Cm²] | Q_{dl} | | R_{ct} [Ω Cm²] | R_L [Ω Cm²] | L [kH cm⁻²] |
		Yo [μΩ⁻¹ cm⁻² sⁿ]	n		Yo [μΩ⁻¹ cm⁻² sⁿ]	n			
B	1.2 ± 0.4	10 472.1 ± 107	0.931 ± 0.03	191 ± 14	786.3 ± 24	0.945 ± 0.01	326 ± 27	—	—
C	1.2 ± 0.3	1013.4 ± 94	0.906 ± 0.04	162 ± 33	758.8 ± 39	0.947 ± 0.03	407 ± 14	—	—
M	1.9 ± 0.2	—	—	—	890.3 ± 54	0.981 ± 0.04	510 ± 54	231 ± 34	16.06 ± 11
SY	1.5 ± 0.3	—	—	—	599.9 ± 12	0.721 ± 0.02	2092 ± 92	541 ± 31	462.7 ± 9
SY 3 days	0.8 ± 0.1	—	—	—	519.6 ± 32	0.888 ± 0.01	1863 ± 91	461 ± 22	143.9 ± 12
SY 7 days	1.1 ± 0.3	—	—	—	359.7 ± 43	0.910 ± 0.03	1573 ± 72	214 ± 42	139.7 ± 14
SY 15 days	1.4 ± 0.2	199.5 ± 12	0.365 ± 0.01	239 ± 34	531.1 ± 27	0.971 ± 0.01	828 ± 31	—	—

range. For aluminium alloys, this time constant with low impedance typically represents the formation of corrosion products at the metal surface.[77,89] Visual inspection clearly indicated that B, M and C were corroded after 3 days of immersion and the corrosion products were observed on the metal surface. In addition, the adsorption process related to the presence of melamine seems insufficient to offer corrosion protection to AA2024. On the other hand, SY sample continues to offer corrosion protection to AA2024 over a longer period of immersion, 15 days, as indicated by Fig. 6. The inductive behaviour at low frequency decreases with immersion time and finally, after 15 days, a capacitive behaviour is observed instead of that inductive one. Although, the total impedance of the SY sample decreases gradually with immersion time, visual inspection clearly indicated that there is no corrosion products on the sample surface. Also, the optical observation of SY sample (not presented) showed yellowish stains which may accompany the presence of the cerium inhibitive layer on the metal surface.[90,91] This behaviour suggests that the initial inductive loop was not related to the corrosion process.

The EIS experimental data was fitted to equivalent electrical circuits and all EIS parameters were calculated. The circuit shown in Fig. 7a was used to fit the experimental results of melamine and SY sample during the immersion in the corrosive solution in the first week of immersion period, while the circuit presented in Fig. 7b was used to fit the data for immersion periods beyond 1 week. The circuit in Fig. 7b was also used to fit the experimental result of the blank and cerium-only samples. A constant phase element (Q) is used instead of pure capacitance due to the porous corrosion products and surface roughness.[92,93] In the circuits shown, R_s represents the solution

electrical resistance, R_{ct} is the charge transfer resistance, Q_{dl} is the double layer capacitance, R_L is the inductance resistance, L is the inductance element, R_c is the resistance of the layer formed on the metal surface and Q_C is the layer capacitance. The layer formed in the case of the SY sample is considered to be a protective layer, while in the case of B, and C samples this layer is considered to be corrosion products. The fitting results of the Nyquist plots are listed in Table 2. It can be noticed that the charge transfer resistance of SY sample is much greater than that of B, C, or M samples after 24 h of immersion in the NaCl corrosive electrolyte. Also, the charge transfer resistance of SY sample decreased with time of immersion indicating the decrease of corrosion protective performance for the AA2024 substrate. This behaviour may be due to the long immersion term with low inhibitor concentration. The capacitive behaviour of the double layer capacitance did not significantly change (n closes to unity).

From the above discussion, it is concluded that melamine or Ce^{4+}, in isolation, does not offer corrosion protection for AA2024 in artificial sea water. Although SY contains the same amount of cerium as the C sample and the same amount of melamine as the M sample, the combination of M + C significantly decreases the corrosion rate of AA2024 in 3.5% NaCl solution, confirming the synergistic effect.

3.2 Surface analysis

Fig. 8 depicts the appearance of a blank aluminium sample surface after 72 h of immersion in the 3.5% NaCl electrolyte. The image and EDX analysis clearly show pitting corrosion around the IMP containing copper, magnesium and iron. The pitting (arrowed) comprises dissolution of aluminium matrix
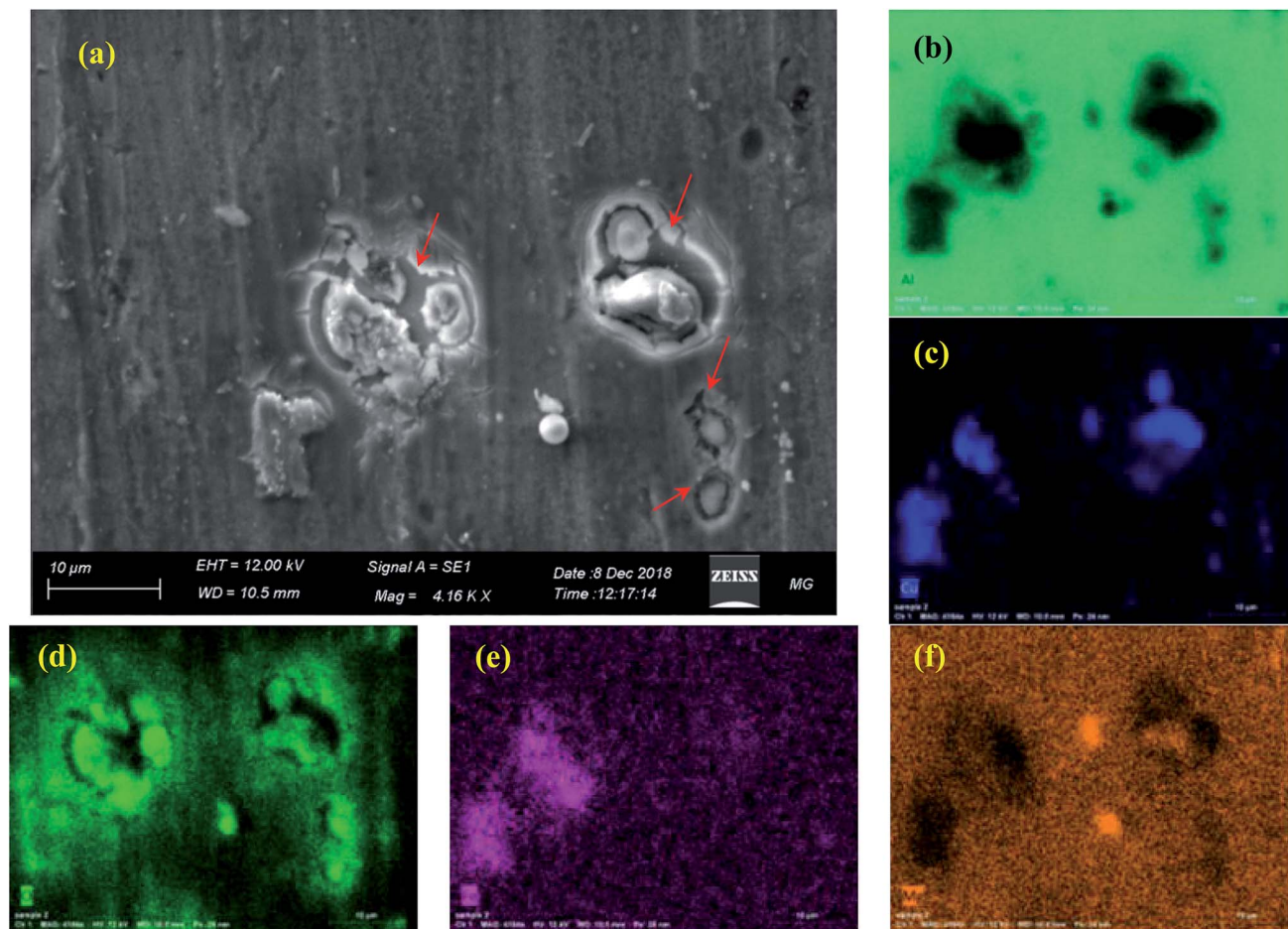
Fig. 8 (a) SEM image with corresponding (b) Al, (c) Cu, (d) O, (e) Fe and (f) Mg EDX maps. of the blank sample after 72 h immersion in 3.5% NaCl at room temperature.

around IMP containing copper, which are cathodic with respect to the aluminium matrix.

Fig. 9 illustrates the SEM images of AA2024 after immersion in NaCl electrolyte in the present of melamine and ceric sulphate separately. The images demonstrate that both of sample surfaces show pitting corrosion covering the entire surface (arrows). These results indicate that each of Ce^{4+} and melamine, in isolation, cannot protect AA2024 in a neutral NaCl solution, confirming the electrochemical results.

Fig. 10 illustrates the SEM analysis of the SY sample, which clearly shows that there is negligible sign of localized corrosion on the aluminium surface after 72 h of immersion in the corrosive electrolyte. The SY inhibitor provides higher corrosion protection to AA2024 when compared to that of the blank,
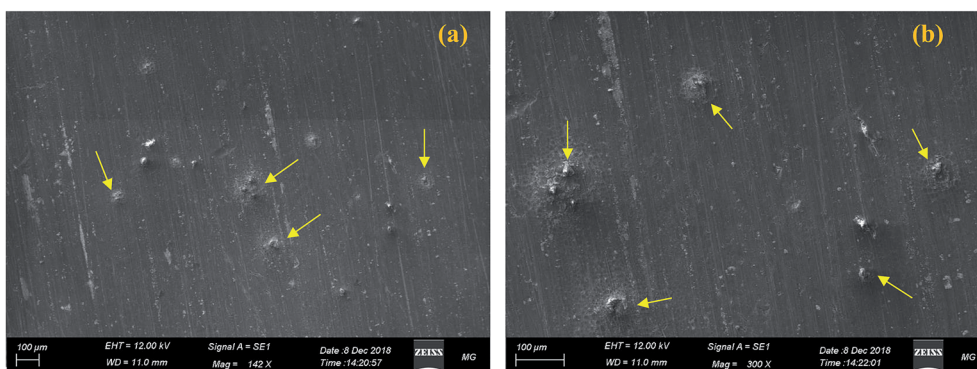

Fig. 9 SEM images of AA2024 after 72 h immersion in 3.5% NaCl containing 5 ppm of (a) C and (b) M.
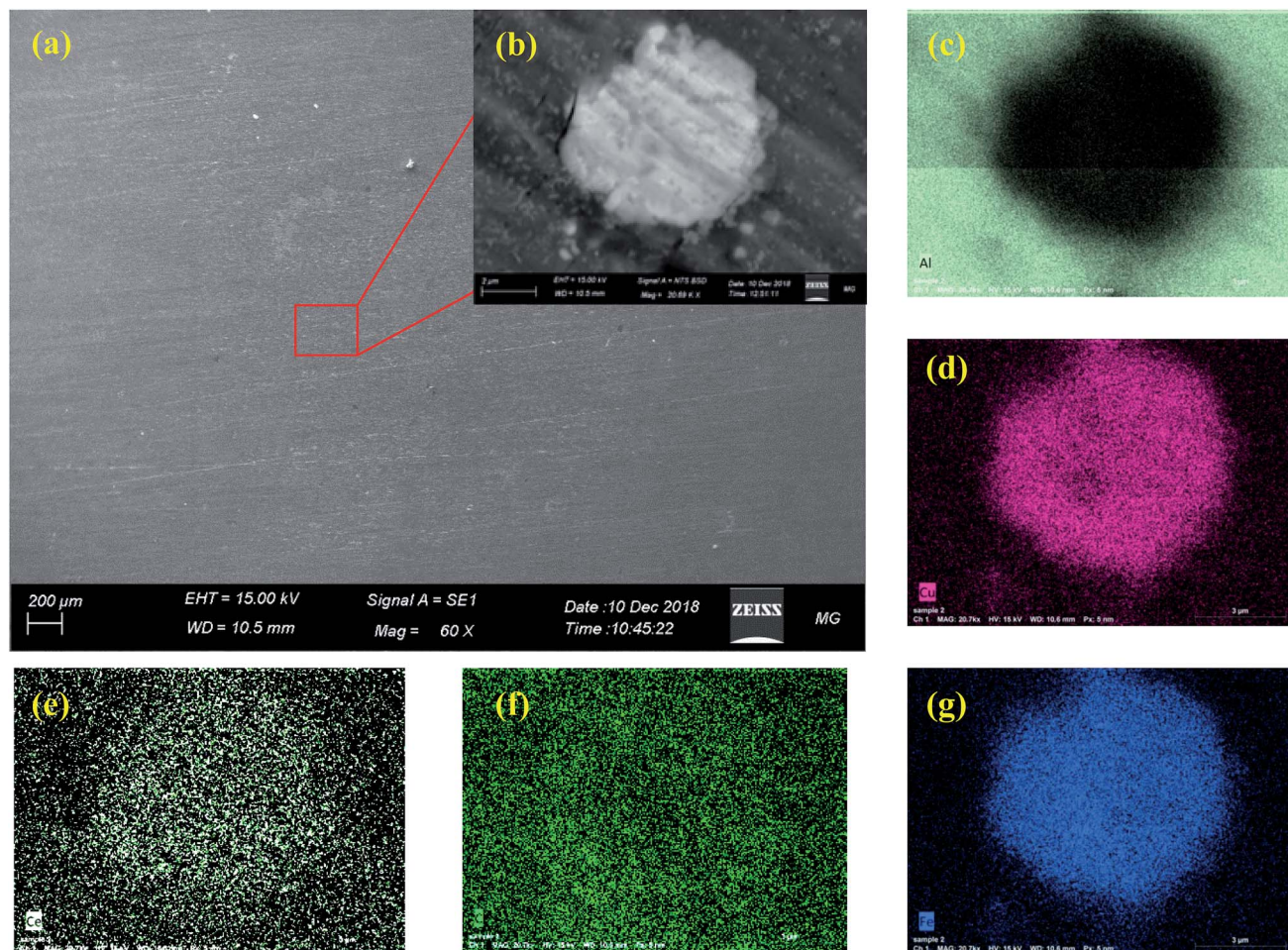
Fig. 10 SEM images of SY sample (a) low and (b) high magnification, with corresponding (c) Al, (d) Cu, (e) O, (f) Fe and (g) Mg EDX mapping after 72 h immersion in 3.5% NaCl at room temperature.

melamine and ceric sulphate samples which confirms the results of the electrochemical techniques. Also, the EDX mapping of a high magnification back scatter image of an IMP, Fig. 10b, depicts that it contains copper, iron, carbon and cerium as indicated by Fig. 10c–g. Also, it does not show any sign of localized corrosion due to the deposition of cerium on this spot. This IMP with a high content of copper would be

cathodic with respect to the aluminium matrix. Also, the EDX map of cerium seems to be identical as that of copper. The presence of copper as the main alloying elements of AA2024 enhances the nucleation and precipitation of cerium on cathodic sites.[94] These results confirm that cerium acts as a cathodic inhibitor and are in a good agreement with the potentiodynamic polarization results. Also, EDX mapping
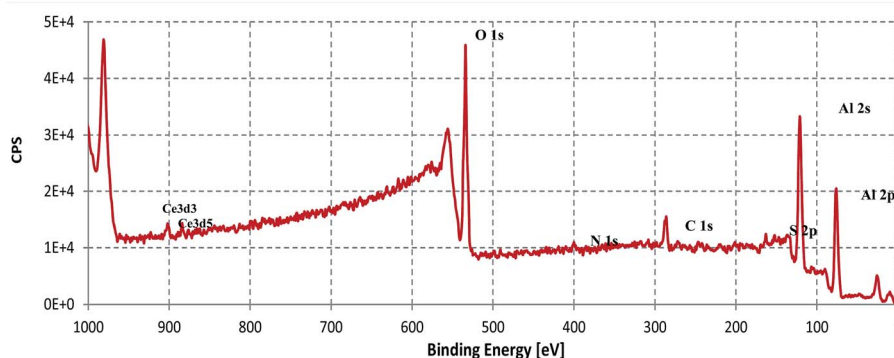

Fig. 11 XPS survey scan of the SY sample immersed in 3.5% NaCl for 48 h at room temperature.
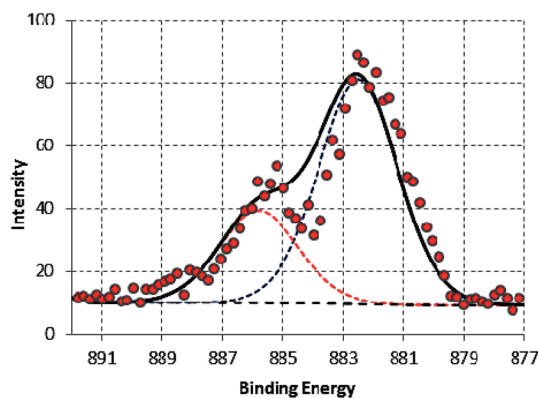
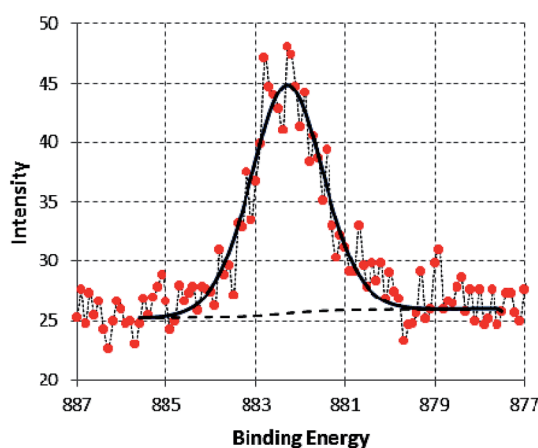**Fig. 12** High-resolution XPS Ce 3d5 of SY sample after 48 h immersion in 3.5% NaCl at room temperature.

Fig. 13 High-resolution XPS Ce 3d5 of Ce(SO$_4$)$_2$ powder.

shows that the carbon appears mainly around the IMP where the main source of this carbon is the melamine. These results indicate that Ce and melamine do not cover the exact same area indicating they are not in the same molecule.

3.3 Corrosion mechanism

3.3.1 XPS study. Determination of the oxidation state of the precipitated cerium on the substrate surface is key to understanding the mechanism of corrosion inhibition. In this respect, XPS is a suitable tool to study the cerium oxidation state at the metal surface.

The XPS survey scan of the SY sample immersed in 3.5% NaCl for 48 h, at room temperature, is shown in Fig. 11. The figure contains Al, O, C, N, Ce and S.

A high-resolution spectrum of the Ce 3d peak is shown in Fig. 12. The overall envelope indicates that it contains two components located at 885.8 ± 0.2 eV and 882.6 ± 0.2 eV corresponding to Ce^{3+} and Ce^{4+} (ref. 40, 47 and 95) with 31.1% Ce^{3+}. To investigate the source of Ce^{3+}, XPS analysis was applied for the raw source of cerium, Ce(SO$_4$)$_2$. The corresponding high-resolution spectra of Ce 3d is illustrated in Fig. 13. The spectra clearly shows a single component at 882.5 ± 0.2 which
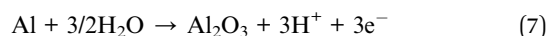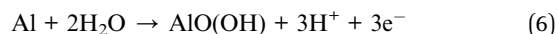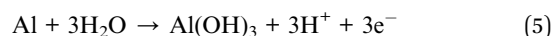
corresponding to Ce^{4+}. These results confirm that Ce^{4+} reduces to Ce^{3+} in this corrosive electrolyte containing melamine besides the metal substrate. This result is consistent with the findings of Matter et al.[41] although, the authors did not point to the reduction reaction of Ce^{4+} to form Ce^{3+}.

3.3.2 Corrosion of AA2024. Generally, the corrosion mechanism of copper–aluminium alloys, 2xxx series, is predominantly influenced by the presence of IMPs. Cu-containing alloys such as AA2024 are subjected localized corrosion in solutions that contains Cl$^-$ as a result of the presence of, for instance; AlCuMnFe, Al$_2$CuMg and AlCu$_2$, each having a different corrosion potential to that of the aluminium matrix. The shape and size of the localized pitting, varies according to the nature and size of these IMPs.[3] Inclusions with particle size >1 μm are not only responsible for initiating pitting corrosion, but they also do not contribute to the mechanical properties of the alloys.[4,44,96,97]

In aerated NaCl solution, the oxygen reduction reaction (low over-potentials) governs the cathode process of an AA2024 sample (eqn (3)), being the electron acceptor reaction from the oxidation of the metal (eqn (4));

$$O_2 + 2H_2O + 4e^- \rightarrow 4OH^- \tag{3}$$

$$Al \rightarrow 3e^- + Al^{3+} \tag{4}$$
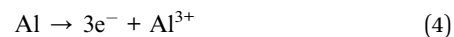
Dissolution of the aluminium matrix, in Cl$^-$ containing solutions, occurs through a series of oxidation reactions producing a Al(OH)Cl$^+$ complex which is dissolved in such aqueous solution as follows;

$$Al + 3H_2O \rightarrow Al(OH)_3 + 3H^+ + 3e^- \tag{5}$$

$$Al + 2H_2O \rightarrow AlO(OH) + 3H^+ + 3e^- \tag{6}$$

$$Al + 3/2H_2O \rightarrow Al_2O_3 + 3H^+ + 3e^- \tag{7}$$

$$Al(OH)^{+2} + Cl^- \rightarrow Al(OH)Cl^+ + 3H^+ + 3e^- \tag{8}$$

IMP provide the cathodic sites at which the oxygen reduction reactions occur. The matrix adjacent to the IPM is the site at which pitting corrosion takes place. Therefore the key to an effective inhibition is to hinder or stop one or both of the cathodic and anodic reactions.

3.3.3 Proposed mechanism. In the case of corrosion inhibition by an active organic component with Ce^{4+}, two mechanisms of corrosion prevention are suggested:

(1) A complex is formed between the organic component and Ce^{4+} via vacant orbital filling. In this mechanism, the complex is adsorbed on the metal substrate to hinder both cathodic and anodic reactions. In this case the inhibitor would be of a mixed type inhibitor.

(2) The second mechanism is a reduction reaction of Ce^{4+} to form Ce^{3+} (eqn (9)), which takes place within 24 h.[47,98] It is acceptable to assume that the anodic reaction is the oxidation of aluminium matrix (eqn (4)).[99] The formed Ce^{3+} in turn reacts to form a thin hydroxide layer of Ce^{3+} (eqn (10)). H$_2$O$_2$ is formed as an intermediate of oxygen reduction, (eqn (11a)) from which
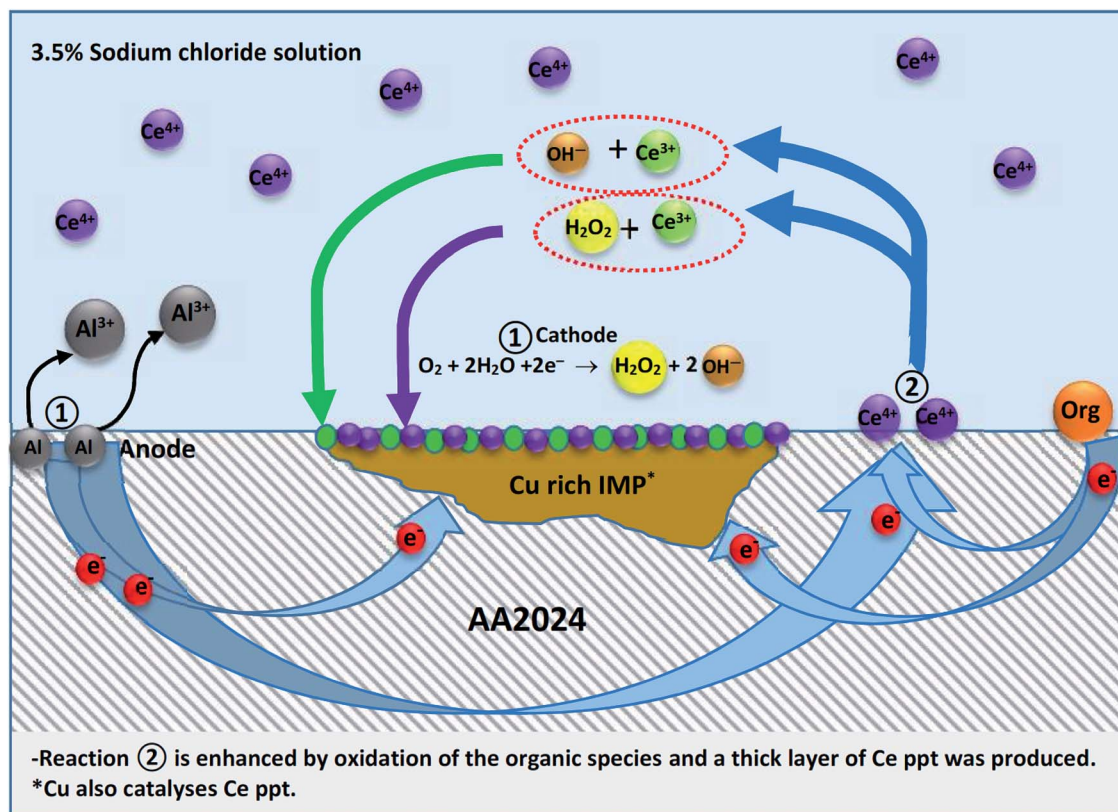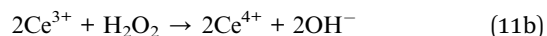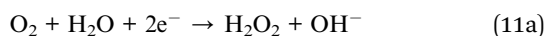
Fig. 14 Proposed corrosion protection mechanism of Ce^{4+}/organic inhibitor for AA2024.

Ce^{4+} precipitation at the cathodic IMP sites occurs (eqn (11b)).[41,99] This thin cerium salt layer does not appear to be sufficient to achieve corrosion protection *via* inhibiting the cathodic reactions. When another compound susceptible to oxidation reaction is present (such as melamine and the other previously used compounds: vanillin, iso-vanillin, sodium oleate and 3,4-dihydroxybenzaldehye) more electrons are offered to enhance the reduction of Ce^{4+} forming a thicker layer of cerium precipitate protecting the metal surface. In this case, cathodic type inhibitor is predominant.

$$Ce^{4+} + e^- \rightarrow Ce^{3+} \qquad (9)$$

$$Ce^{3+} + 3OH^- \rightarrow Ce(OH)_3 \qquad (10)$$

$$O_2 + H_2O + 2e^- \rightarrow H_2O_2 + OH^- \qquad (11a)$$

$$2Ce^{3+} + H_2O_2 \rightarrow 2Ce^{4+} + 2OH^- \qquad (11b)$$

Both mechanisms are valid and the predominant mechanism may depend on the total concentration of the inhibitor (organic component and Ce^{4+}), the organic component/Ce^{4+} ratio and the pH.

In the present case, the total concentration of the inhibitor is limited to 10 ppm, and the organic component/Ce^{4+} ratio is 1 : 1. Also, the SY (Ce^{4+}/melamine) sample clearly showed superior protection for AA2024 where cerium precipitation was observed at the cathodic sites. In addition, the PDP results

showed that SY is predominantly a cathodic inhibitor. Further, EIS indicated that the SY sample may exhibit a redox reaction(s) during immersion of AA2024 in the aerated NaCl solution. In the same context, this redox activity does not appear in the absence of melamine indicating that melamine facilitates the redox process. This process was reflected in the XPS analysis where, it showed Ce^{3+} at the SY sample surface. Therefore, the second corrosion prevention mechanism, discussed above, seems to be predominant and the mechanism is displayed in Fig. 14.

The mechanism of protection AA2024 in the presence of both Ce^{4+} and melamine can be summarized as follows; Ce^{3+} is produced from a set of complicated reduction reaction(s) of Ce^{4+} that is improved in the presence of melamine. Melamine can not only be oxidized[100,101] but also can be used as a structure-director and stabilizing agent[102] during the precipitation of cerium on the metal surface. In addition, its molecule contains 6 nitrogen atoms than enhances the chance of adsorption on the aluminium substrate. Furthermore the copper rich IMP also catalyses cerium salts precipitation on the cathodic sites.

4. Conclusions

PDP and EIS has shown that the combination of Ce^{4+} and melamine can offer a synergistic effect for the corrosion prevention of AA2024 in aerated 3.5% NaCl solution. PDP also

indicates that this combination acts as a cathodic inhibitor and EIS results confirm the PDP data. The SEM results along with optical observation indicate that melamine and Ce^{4+}, individually, cannot offer suitable corrosion prevention for AA2024 in this NaCl electrolyte. For the 1 : 1 melamine: Ce^{4+} sample, the EDX mapping showed that cerium compounds were precipitated at the cathodic IMP sites on the metal surface leading to an inhibition of the oxygen reduction reaction. The XPS revealed that Ce^{4+} was reduced to Ce^{3+} in the presence of melamine, this step is considered crucial in the proposed protection mechanism.

Conflicts of interest

There are no conflicts to declare.

References

1 C. Vargel, *Corrosion of aluminium*, Elsevier, 2004.

2 J. K. Wessel, *The handbook of advanced materials: enabling new designs*, John Wiley & Sons, 2004.

3 G. Chen, M. Gao and R. Wei, Microconstituent-induced pitting corrosion in aluminum alloy 2024-T3, *Corrosion*, 1996, **52**(1), 8–15.

4 B. Chambers and S. Taylor, The high throughput assessment of aluminium alloy corrosion using fluorometric methods. Part II–A combinatorial study of corrosion inhibitors and synergistic combinations, *Corros. Sci.*, 2007, **49**(3), 1597–1609.

5 J. G. Brunner, *et al.*, Impact of ultrafine-grained microstructure on the corrosion of aluminium alloy AA2024, *Corros. Sci.*, 2012, **57**, 209–214.

6 D. Ho, *et al.*, Cerium dibutylphosphate as a corrosion inhibitor for AA2024-T3 aluminum alloys, *J. Electrochem. Soc.*, 2006, **153**(9), B392–B401.

7 R. Akid, M. Gobara and H. Wang, Corrosion protection performance of novel hybrid polyaniline/sol–gel coatings on an aluminium 2024 alloy in neutral, alkaline and acidic solutions, *Electrochim. Acta*, 2011, **56**(5), 2483–2492.

8 L. Coelho, D. Cossement and M.-G. Olivier, Benzotriazole and cerium chloride as corrosion inhibitors for AA2024-T3: An EIS investigation supported by SVET and ToF-SIMS analysis, *Corros. Sci.*, 2018, **130**, 177–189.

9 M. L. Zheludkevich, *et al.*, Triazole and thiazole derivatives as corrosion inhibitors for AA2024 aluminium alloy, *Corros. Sci.*, 2005, **47**(12), 3368–3383.

10 S. V. Lamaka, *et al.*, High effective organic corrosion inhibitors for 2024 aluminium alloy, *Electrochim. Acta*, 2007, **52**(25), 7231–7247.

11 T. Hu, *et al.*, A localized approach to study corrosion inhibition of intermetallic phases of AA 2024-T3 by cerium malate, *Appl. Surf. Sci.*, 2019, **467**, 1011–1032.

12 B. Prakashaiah, *et al.*, Corrosion inhibition of 2024-T3 aluminum alloy in 3.5% NaCl by thiosemicarbazone derivatives, *Corros. Sci.*, 2018, **136**, 326–338.

13 E. Kalman, I. Lukovits and G. Palinkas, A simple model of synergism of corrosion inhibitors, *ACH - Models Chem.*, 1993, **132**(4), 527–537.

14 G. N. Mu, X. Li and F. Li, Synergistic inhibition between o-phenanthroline and chloride ion on cold rolled steel corrosion in phosphoric acid, *Mater. Chem. Phys.*, 2004, **86**(1), 59–68.

15 G. Mu, X. Li and G. Liu, Synergistic inhibition between tween 60 and NaCl on the corrosion of cold rolled steel in 0.5 M sulfuric acid, *Corros. Sci.*, 2005, **47**(8), 1932–1952.

16 K. Aramaki, Synergistic inhibition of zinc corrosion in 0.5 M NaCl by combination of cerium(III) chloride and sodium silicate, *Corros. Sci.*, 2002, **44**(4), 871–886.

17 R. Solmaz, *et al.*, The investigation of synergistic inhibition effect of rhodanine and iodide ion on the corrosion of copper in sulphuric acid solution, *Corros. Sci.*, 2011, **53**(10), 3231–3240.

18 H. Gao, *et al.*, High efficiency corrosion inhibitor 8-hydroxyquinoline and its synergistic effect with sodium dodecylbenzenesulphonate on AZ91D magnesium alloy, *Corros. Sci.*, 2010, **52**(5), 1603–1609.

19 L. Guo, *et al.*, Theoretical insight into an empirical rule about organic corrosion inhibitors containing nitrogen, oxygen, and sulfur atoms, *Appl. Surf. Sci.*, 2017, **406**, 301–306.

20 L. M. Vračar and D. Dražić, Adsorption and corrosion inhibitive properties of some organic molecules on iron electrode in sulfuric acid, *Corros. Sci.*, 2002, **44**(8), 1669–1680.

21 M. Gobara, A. Baraka and B. Zaghloul, Inhibition of mild steel corrosion in sulfuric acid solution using collagen, *Res. Chem. Intermed.*, 2015, **41**(10), 7245–7261.

22 M. Arenas, A. Conde and J. De Damborenea, Cerium: a suitable green corrosion inhibitor for tinplate, *Corros. Sci.*, 2002, **44**(3), 511–520.

23 Z. Mahidashti, T. Shahrabi and B. Ramezanzadeh, The role of post-treatment of an ecofriendly cerium nanostructure Conversion coating by green corrosion inhibitor on the adhesion and corrosion protection properties of the epoxy coating, *Prog. Org. Coat.*, 2018, **114**, 19–32.

24 N. Nam, *et al.*, Role of hydroxyl group in cerium hydroxycinnamate on corrosion inhibition of mild steel in 0.6 M NaCl solution, *J. Saudi Chem. Soc.*, 2019, **23**(1), 30–42.

25 M. Dabalà, *et al.*, Cerium-based conversion layers on aluminum alloys, *Appl. Surf. Sci.*, 2001, **172**(3–4), 312–322.

26 S. Taylor and B. Chambers, Identification and characterization of nonchromate corrosion inhibitor synergies using high-throughput methods, *Corrosion*, 2008, **64**(3), 255–270.

27 M. Bethencourt, *et al.*, Lanthanide compounds as environmentally-friendly corrosion inhibitors of aluminium alloys: a review, *Corros. Sci.*, 1998, **40**(11), 1803–1819.

28 K. Yasakau, *et al.*, Cerium molybdate nanowires for active corrosion protection of aluminium alloys, *Corros. Sci.*, 2012, **58**, 41–51.

29 X. Jiang, R. Guo and S. Jiang, Evaluation of self-healing ability of Ce–V conversion coating on AZ31 magnesium alloy, *J. Magnesium Alloys*, 2016, **4**(3), 230–241.

30 E. Saei, *et al.*, Effects of combined organic and inorganic corrosion inhibitors on the nanostructure cerium based conversion coating performance on AZ31 magnesium alloy: Morphological and corrosion studies, *Corros. Sci.*, 2017, **127**, 186–200.

31 Y. Zhu, *et al.*, Research on anti-corrosion property of rare earth inhibitor for X70 steel, *J. Rare Earths*, 2013, **31**(7), 734–740.

32 K. Aramaki, Cerium (III) chloride and sodium octylthiopropionate as an effective inhibitor mixture for zinc corrosion in 0.5 M NaCl, *Corros. Sci.*, 2002, **44**(6), 1361–1374.

33 J. Liu, *et al.*, Synergism between cerium nitrate and sodium dodecylbenzenesulfonate on corrosion of AA5052 aluminium alloy in 3 wt.% NaCl solution, *Appl. Surf. Sci.*, 2016, **389**, 369–377.

34 M. Ramezanzadeh, *et al.*, Highly effective inhibition of mild steel corrosion in 3.5% NaCl solution by green Nettle leaves extract and synergistic effect of eco-friendly cerium nitrate additive: Experimental, MD simulation and QM investigations, *J. Mol. Liq.*, 2018, **256**, 67–83.

35 M. Forsyth, *et al.*, Inhibition of corrosion on AA2024-T3 by new environmentally friendly rare earth organophosphate compounds, *Corrosion*, 2008, **64**(3), 191–197.

36 D.-Q. Zhang, H. Wu and L.-X. Gao, Synergistic inhibition effect of l-phenylalanine and rare earth Ce (IV) ion on the corrosion of copper in hydrochloric acid solution, *Mater. Chem. Phys.*, 2012, **133**(2–3), 981–986.

37 X. Li, *et al.*, Synergistic inhibition effect of rare earth cerium (IV) ion and anionic surfactant on the corrosion of cold rolled steel in H_2SO_4 solution, *Corros. Sci.*, 2008, **50**(9), 2635–2645.

38 X. Li, *et al.*, The synergistic inhibition effect of rare earth cerium (IV) ion and iso-vanillin on the corrosion of cold rolled steel in 1.0 M H_2SO_4 solution, *Mater. Lett.*, 2007, **61**(11–12), 2514–2517.

39 X. Li, *et al.*, Synergistic inhibition effect of rare earth cerium (IV) ion and sodium oleate on the corrosion of cold rolled steel in phosphoric acid solution, *Corros. Sci.*, 2010, **52**(4), 1167–1178.

40 X. Li, *et al.*, Synergism between rare earth cerium (IV) ion and vanillin on the corrosion of cold rolled steel in 1.0 M HCl solution, *Corros. Sci.*, 2008, **50**(12), 3599–3609.

41 E. Matter, *et al.*, Comparison between the inhibition efficiencies of Ce (III) and Ce (IV) ammonium nitrates against corrosion of AA2024 aluminum alloy in solutions of low chloride concentration, *Corros. Sci.*, 2012, **62**, 22–33.

42 A. Davenport, H. Isaacs and M. Kendig, X-Ray absorption study of cerium in the passive film on aluminum, *J. Electrochem. Soc.*, 1989, **136**(6), 1837–1838.

43 A. Davenport, H. Isaacs and M. Kendig, XANES investigation of the role of cerium compounds as corrosion inhibitors for aluminum, *Corros. Sci.*, 1991, **32**(5–6), 653–663.

44 K. A. Yasakau, *et al.*, Mechanism of corrosion inhibition of AA2024 by rare-earth compounds, *J. Phys. Chem. B*, 2006, **110**(11), 5515–5528.

45 B. Hinton, Corrosion inhibition with rare earth metal salts, *J. Alloys Compd.*, 1992, **180**(1–2), 15–25.

46 M. Jakab, F. Presuel-Moreno and J. Scully, Effect of molybdate, cerium, and cobalt ions on the oxygen reduction reaction on AA2024-T3 and selected intermetallics experimental and modeling studies, *J. Electrochem. Soc.*, 2006, **153**(7), B244–B252.

47 J. Sánchez-Amaya, *et al.*, XPS and AES analyses of cerium conversion coatings generated on AA5083 by thermal activation, *Surf. Coat. Technol.*, 2012, **213**, 105–116.

48 M. Jakab, F. Presuel-Moreno and J. Scully, Critical concentrations associated with cobalt, cerium, and molybdenum inhibition of AA2024-T3 corrosion: Delivery from Al-Co-Ce (-Mo) alloys, *Corrosion*, 2005, **61**(3), 246–263.

49 X. Li, *et al.*, Synergism between rare earth cerium (IV) ion and vanillin on the corrosion of steel in H_2SO_4 solution: Weight loss, electrochemical, UV–vis, FTIR, XPS, and AFM approaches, *Appl. Surf. Sci.*, 2008, **254**(17), 5574–5586.

50 X. Li, *et al.*, Synergistic inhibition effect of rare earth cerium (IV) ion and 3, 4-dihydroxybenzaldehye on the corrosion of cold rolled steel in H_2SO_4 solution, *Corros. Sci.*, 2009, **51**(11), 2639–2651.

51 X. Li, *et al.*, The synergistic inhibition effect of rare earth cerium(IV) ion and iso-vanillin on the corrosion of cold rolled steel in 1.0 M H_2SO_4 solution, *Mater. Lett.*, 2007, **61**(11), 2514–2517.

52 G.-N. Mu, *et al.*, Synergistic effect on corrosion inhibition by cerium (IV) ion and sodium molybdate for cold rolled steel in hydrochloric acid solution, *Acta Chim. Sin.*, 2004, **62**(24), 2386–2390.

53 S. A. Umoren and M. M. Solomon, Synergistic corrosion inhibition effect of metal cations and mixtures of organic compounds: a review, *J. Environ. Chem. Eng.*, 2017, **5**(1), 246–273.

54 T. P. Jose, S. T. Nandibewoor and S. M. Tuwar, Kinetics and mechanism of the oxidation of vanillin by hexacyanoferrate (III) in aqueous alkaline medium, *J. Solution Chem.*, 2006, **35**(1), 51–62.

55 C. Fargues, *et al.*, Kinetics of vanillin oxidation, *Chem. Eng. Technol.*, 1996, **19**(2), 127–136.

56 D. S. Munavalli, S. A. Chimatadar and S. T. Nandibewoor, Oxidation of vanillin by a new oxidant diperiodatoargentate (III) in aqueous alkaline medium, *Ind. Eng. Chem. Res.*, 2007, **46**(5), 1459–1464.

57 Y. Zhang, *et al.*, Facile synthesis of V^{4+} self-doped,[010] oriented $BiVO_4$ nanorods with highly efficient visible light-induced photocatalytic activity, *Phys. Chem. Chem. Phys.*, 2014, **16**(44), 24519–24526.

58 Y. Sun, *et al.*, Highly efficient visible-light-driven photocatalytic activities in synthetic ordered monoclinic $BiVO_4$ quantum tubes–graphene nanocomposites, *Nanoscale*, 2012, **4**(12), 3761–3767.

59 H. Li, *et al.*, Synthesis and characterization of monoclinic $BiVO_4$ nanorods and nanoplates *via* microemulsion-

mediated hydrothermal method, *Phys. E*, 2011, **43**(7), 1323–1328.

60 N. Ermiş, L. Uzun and A. Denizli, Preparation of molecularly imprinted electrochemical sensor for l-phenylalanine detection and its application, *J. Electroanal. Chem.*, 2017, **807**, 244–252.

61 X. Li, *et al.*, Synergism between protocatechualdehyde and rare earth cerium (IV) ion on the corrosion of cold rolled steel in hydrochloric acid solution, *Mater. Corros.*, 2010, **61**(3), 229–237.

62 D. Nematollahi and S. Golabi, Investigation of the electro-methoxylation reaction: Part 1. Electrochemical study of 4-tert-butylcatechol and 3,4-dihydroxybenzaldehyde in methanol, *J. Electroanal. Chem.*, 2000, **481**(2), 208–214.

63 M. Lutter, *et al.*, Oxidation of caffeic acid in a wine-like medium: Production of dihydroxybenzaldehyde and its subsequent reactions with (+)-catechin, *Food Chem.*, 2007, **105**(3), 968–975.

64 M. F. Delbem, W. J. Baader and S. H. P. Serrano, Mechanism of 3,4-dihydroxybenzaldehyde electropolymerization at carbon paste electrodes: catalytic detection of NADH, *Quim. Nova*, 2002, **25**(5), 741–747.

65 M. Sugumaran, Oxidation of 3,4-Dihydroxybenzylamine Affords 3,4-Dihydroxybenzaldehyde *via* the Quinone Methide Intermediate, *Pigm. Cell Res.*, 1995, **8**(5), 250–254.

66 H. M. A. El-Lateef, Synergistic effect of polyethylene glycols and rare earth Ce^{4+} on the corrosion inhibition of carbon steel in sulfuric acid solution: electrochemical, computational, and surface morphology studies, *Res. Chem. Intermed.*, 2016, **42**(4), 3219–3240.

67 A. M. Sakharov, L. I. Mazaletskaya and I. P. Skibida, Catalytic Oxidative Deformylation of Polyethylene Glycols with the Participation of Molecular Oxygen, *Kinet. Catal.*, 2001, **42**(5), 662–668.

68 F. Kawai, Biodegradation of polyethers (polyethylene glycol, polypropylene glycol, polytetramethylene glycol, and others), *Biopolymers Online*, 2005, **9**.

69 D. Mantzavinos, *et al.*, Wet air oxidation of polyethylene glycols; mechanisms, intermediates and implications for integrated chemical-biological wastewater treatment, *Chem. Eng. Sci.*, 1996, **51**(18), 4219–4235.

70 J. Haines and M. Alexander, Microbial degradation of polyethylene glycols, *Appl. Environ. Microbiol.*, 1975, **29**(5), 621–625.

71 D. F. Dwyer and J. M. Tiedje, Degradation of ethylene glycol and polyethylene glycols by methanogenic consortia, *Appl. Environ. Microbiol.*, 1983, **46**(1), 185–190.

72 S. Nagarajan, K. Srinivasan and K. V. Rao, Kinetic and mechanistic studies on the oxidation of poly (ethylene glycol) by ceric sulphate in sulphuric acid medium, *Polym. J.*, 1994, **26**(7), 851.

73 J. K. Szymański, F. Temprano-Coleto and J. Pérez-Mercader, Unusual kinetics of poly (ethylene glycol) oxidation with cerium (IV) ions in sulfuric acid medium and implications for copolymer synthesis, *Phys. Chem. Chem. Phys.*, 2015, **17**(10), 6713–6717.

74 G. Zellner, H. Kneifel and J. Winter, Oxidation of benzaldehydes to benzoic acid derivatives by three Desulfovibrio strains, *Appl. Environ. Microbiol.*, 1990, **56**(7), 2228–2233.

75 H.-R. Bjørsvik, L. Liguori and F. Minisci, High Selectivity in the Oxidation of Mandelic Acid Derivatives and in O-Methylation of Protocatechualdehyde: New Processes for Synthesis of Vanillin, iso-Vanillin, and Heliotropin, *Org. Process Res. Dev.*, 2000, **4**(6), 534–543.

76 J. Fujita and M. M. Hyland, Polyaniline coatings for aluminium: Preliminary study of bond and anti-corrosion, *Int. J. Mod. Phys. B*, 2003, **17**(08n09), 1164–1169.

77 M. Gobara, *et al.*, Novel Smart Hydroxyapatite/Silica Sol–Gel Nanocomposite Hybrid Coating for Corrosion Protection of AA2024, *J. Inorg. Organomet. Polym. Mater.*, 2018, 1–11.

78 N. K. Gupta, *et al.*, Schiff's bases derived from L-lysine and aromatic aldehydes as green corrosion inhibitors for mild steel: Experimental and theoretical studies, *J. Mol. Liq.*, 2016, **215**, 47–57.

79 A. N. Grassino, *et al.*, Utilization of tomato peel waste from canning factory as a potential source for pectin production and application as tin corrosion inhibitor, *Food Hydrocolloids*, 2016, **52**, 265–274.

80 L. Boucherit, *et al.*, Synthesis, characterization and the inhibition activity of 3-(4-cyanophenylazo)-2,4-pentanedione (L) on the corrosion of carbon steel, synergistic effect with other halide ions in 0.5 M H_2SO_4, *J. Mol. Struct.*, 2019, **1177**, 371–380.

81 P. Han, *et al.*, Synergistic effect of mixing cationic and nonionic surfactants on corrosion inhibition of mild steel in HCl: Experimental and theoretical investigations, *J. Colloid Interface Sci.*, 2018, **516**, 398–406.

82 A. Singh and M. A. Quraishi, The extract of Jamun (Syzygium cumini) seed as green corrosion inhibitor for acid media, *Res. Chem. Intermed.*, 2013, 1–14.

83 M. A. Amin and M. M. Ibrahim, Corrosion and corrosion control of mild steel in concentrated H_2SO_4 solutions by a newly synthesized glycine derivative, *Corros. Sci.*, 2011, **53**(3), 873–885.

84 U. Donatus, *et al.*, The effect of manufacturing process induced near-surface deformed layer on the corrosion behaviour of AA2198-T851 Al–Cu–Li alloy, *Corros. Eng., Sci. Technol.*, 2019, **54**(3), 205–215.

85 E. Chassaing, M. Joussellin and R. Wiart, The kinetics of nickel electrodeposition: Inhibition by adsorbed hydrogen and anions, *J. Electroanal. Chem. Interfacial Electrochem.*, 1983, **157**(1), 75–88.

86 A. K. Singh and M. A. Quraishi, Effect of Cefazolin on the corrosion of mild steel in HCl solution, *Corros. Sci.*, 2010, **52**(1), 152–160.

87 E. Hür, G. Bereket and Y. Şahin, Corrosion inhibition of stainless steel by polyaniline, poly(2-chloroaniline), and poly (aniline-co-2-chloroaniline) in HCl, *Prog. Org. Coat.*, 2006, **57**(2), 149–158.

88 S. Elbasuney, *et al.*, The significant role of stabilized colloidal ZrO_2 nanoparticles for corrosion protection of

AA2024, *Environmental Nanotechnology, Monitoring & Management*, 2019, **12**, 100242.

89 H. Elgahawi, *et al.*, Eco-friendly corrosion inhibition of AA2024 in 3.5% NaCl using the extract of Linum usitatissimum seeds, *Journal of Bio-and Tribo-Corrosion*, 2017, **3**(4), 55.

90 L. B. Coelho, *et al.*, The corrosion inhibition mechanisms of Ce(III) ions and triethanolamine on graphite—AA2024-T3 galvanic couples revealed by localised electrochemical techniques, *Corros. Sci.*, 2019, **150**, 207–217.

91 J. Carneiro, *et al.*, Chitosan-based self-healing protective coatings doped with cerium nitrate for corrosion protection of aluminum alloy 2024, *Prog. Org. Coat.*, 2012, **75**(1), 8–13.

92 U. Rammelt and G. Reinhard, On the applicability of a constant phase element (CPE) to the estimation of roughness of solid metal electrodes, *Electrochim. Acta*, 1990, **35**(6), 1045–1049.

93 J.-B. Jorcin, *et al.*, CPE analysis by local electrochemical impedance spectroscopy, *Electrochim. Acta*, 2006, **51**(8), 1473–1479.

94 P. Campestrini, *et al.*, Formation of a cerium-based conversion coating on AA2024: relationship with the microstructure, *Surf. Coat. Technol.*, 2004, **176**(3), 365–381.

95 A. Uhart, *et al.*, An Auger and XPS survey of cerium active corrosion protection for AA2024-T3 aluminum alloy, *Appl. Surf. Sci.*, 2016, **390**, 751–759.

96 O. A. Lopez-Garrity, *Corrosion inhibition mechanisms of aluminum alloy 2024-T3 by selected non-chromate inhibitors*, Ohio State University, 2013.

97 R. Buchheit, *et al.*, Local dissolution phenomena associated with S phase (Al_2CuMg) particles in aluminum alloy 2024-T3, *J. Electrochem. Soc.*, 1997, **144**(8), 2621–2628.

98 R. Catubig, *et al.*, The use of cerium and praseodymium mercaptoacetate as thiol-containing inhibitors for AA2024-T3, *Corros. Sci.*, 2014, **81**, 45–53.

99 V. Palanivel, Y. Huang and W. J. van Ooij, Effects of addition of corrosion inhibitors to silane films on the performance of AA2024-T3 in a 0.5 M NaCl solution, *Prog. Org. Coat.*, 2005, **53**(2), 153–168.

100 A. B. Prevot, *et al.*, Degradation of melamine in aqueous systems by vacuum UV-(VUV-) photolysis. An alternative to photocatalysis, *Catal. Today*, 2018.

101 D. Feng, *et al.*, Sensitive detection of melamine by an electrochemiluminescence sensor based on tris (bipyridine) ruthenium (II)-functionalized metal-organic frameworks, *Sens. Actuators, B*, 2018, **265**, 378–386.

102 Q. Liu, *et al.*, One-step melamine-assisted synthesis of graphene-supported AuPt@ Au nanocrystals for enhanced catalytic reduction of p-nitrophenol, *RSC Adv.*, 2015, **5**(116), 96028–96033.